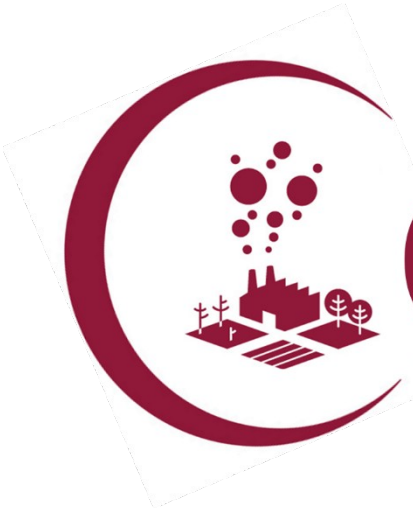

CONFESS

Consistent representation of temporal variations of boundary forcings in reanalyses and seasonal forecasts

Intermediate report WP3

Lauriane Batté

www.confess-h2020.eu

Co-ordinated by ECMWF

CONFESS

Consistent representation of temporal variations of boundary forcings in reanalyses and seasonal forecasts

D3.4 Intermediate report on WP3 activities and results

Author(s): Lauriane Batté (Météo-France)
Andrea Alessandri (ISAC-CNR)
Fransje van Oorschot (ISAC-CNR)
Roberto Bilbao (BSC)
Gildas Dayon (Météo-France)
Retish Senan (ECMWF)
Tim Stockdale (ECMWF)

Dissemination Level:	Public/ Confidential
Date:	26/10/2022
Version:	1.1
Contractual Delivery Date:	31/10/2022
Work Package/ Task:	WP3/ T3.1, T3.2, T3.3
Document Owner:	Météo-France
Contributors:	MF, ISAC-CNR, BSC, ECMWF
Status:	Final

CONFESS

Consistent representation of temporal variations of boundary forcings in reanalyses and seasonal forecasts

Research and Innovation Action (RIA)
H2020- LC-SPACE-18-EO-2020 Copernicus evolution: Research activities in support of the evolution of the Copernicus services - Copernicus Climate Change Service (C3S

Project Coordinator: Dr Magdalena Alonso Balmaseda (ECMWF)
Project Start Date: 01/11/2020
Project Duration: 36 months

Published by the CONFESS Consortium

Contact:
ECMWF, Shinfield Park, Reading, RG2 9AX, United Kingdom
Magdalena.Balmaseda@ecmwf.int

The CONFESS project has received funding from the European Union's Horizon 2020 research and innovation programme under grant agreement No 101004156.

Contents

Figures

Tables

1 Executive Summary

This deliverable provides an overview of work completed or underway in the different tasks of the H2020 CONFESS project Work Package 3 (WP3), dedicated to the evaluation of developments on the temporal variation of vegetation and land-cover (WP1) and aerosols (WP2) in initialised seasonal to multi-annual predictions.

After a brief introduction (Part 2), Part 3 presents progress in evaluating the influence of time-varying land surface boundary conditions and interactive vegetation in sets of experiments run by the three partners involved in this task. Part 4 discusses plans and preliminary results in the impact of volcanic and tropospheric aerosols in seasonal and decadal prediction experiments with the IFS model and EC-Earth. Plans until the completion of the CONFESS project (and final deliverables from this work package) are presented in Part 5.

2 Introduction

2.1 Background

Main objectives of CONFESS WP3 are to integrate developments from the work packages WP1 (dedicated to time-varying vegetation and land cover) and WP2 (dedicated to temporal variation of aerosols) and evaluate these in a seasonal and multi-annual prediction setting, in terms of biases, variability, and changes in the prediction skill at these time scales. The overarching goal of the work package is to provide recommendations for future integration of these model developments in the operational seasonal and multi-annual prediction systems.

Some key developments from WP1 and WP2 have been delivered by partners during the previous months of the project, including the improved representation of vegetation variability (Deliverable 1.2; van Oorschot et al., 2022) and harmonised boundary forcings including Leaf Area Index (Deliverable 1.1; Boussetta and Balsamo, 2021) and tropospheric aerosols (Deliverable 2.1; Stockdale et al., 2022). These developments are at time of writing in the process of being implemented and tested in three different climate prediction systems: IFS coupled to NEMO for the ECMWF seasonal prediction system, CNRM-CM coupled model on which the Météo-France seasonal prediction system is based, and EC-Earth for multi-annual prediction. Another aspect explored is the potential benefit of including interactive vegetation in the seasonal prediction framework.

For some of the developments planned, the main influence expected is not necessarily in terms of skill, but rather related to a better representation of the trends over the re-forecast period and improved consistency of the boundary forcings over the decades for which these re-forecast are run.

2.2 Scope of this deliverable

2.2.1 Objectives of this deliverable

This deliverable is an intermediate report of progress in meeting WP3 objectives. It will therefore address several goals:

- Report on the progress in implementing developments from WP1 and WP2 and running the models in a climate prediction framework;
- Report on preliminary results on the influence of improved land surface;
- Report on preliminary results on the influence of improved aerosols, here focusing on the volcanic aerosols already performed;
- List future plans in preparation of the forthcoming WP3 deliverables.

2.2.2 Work performed in this deliverable

Each partner contributed to this deliverable by sharing the status of ongoing experiments, and preliminary analyses. Work performed built on deliverables from WP1 and WP2 and the experimental protocol designed among partners earlier in the project.

As of now, since each partner has not completed the same sets of experiments, the results presented in this deliverable report mainly on single model analyses. One notable exception is the work on the influence of volcanic aerosol in decadal prediction, which relies on multi-model simulations available through the CMIP6 DCPP component A and component C experimental framework (Bilbao et al., in prep; see section 4.2).

2.2.3 Deviations and counter measures

Some partners have experienced delays in setting up and running the experiments (Milestone 3.2). At ECMWF, delays in implementing the IFS on the new ATOS HPC and the transfer of the data handling system from Reading, UK, to Bologna, Italy, implied that some key data such as the Leaf Area Index data from WP1 were unavailable for several weeks. This, alongside delays and deviations from plan in WP2, has implied that the completion of ECMWF experiments and sharing of data among partners is slightly delayed.

Countermeasures have been implemented to reduce the delay as much as possible. ECMWF worked on setting up the experiments on the ATOS machine and the environment has been prepared as much as possible without access to the data needed to run. The experiments will be run as soon as the HPC and storage environment is fully up and running.

On the other hand, some experiments due for milestone 3.3 in spring 2023 were planned on ATOS but efforts for porting EC-Earth to the new ATOS environment were planned to focus on a more recent version of the model than the one used for the baseline experiments. These new experiments were therefore set up on the ECMWF Cray environment (collaboration between ISAC-CNR and BSC), on which the previous version of EC-Earth was already deployed, and additional resources were allocated to ISAC-CNR so that the experiments could be completed ahead of the original schedule.

3 Impact of land surface forcings on initialised predictions

3.1 Design of initialised prediction experiments

The initialised prediction experiments planned in WP3 to assess the impact of land surface forcings are described in the experimental protocol (Deliverable 3.1, Batté and Stockdale 2021). The following paragraphs present an update from each contributing partner on the realisation of these experiments: ECMWF and Météo-France for the seasonal prediction experiments, and ISAC-CNR for the decadal prediction experiments.

3.1.1 ECMWF

A set of seasonal hindcast experiments covering the historical period 1993-2019 are currently being performed using the ECMWF IFS coupled model. The configuration of these 4-month experiments initialised in May and November is similar to the current operational SEAS5 (Johnson et al., 2019), but with a newer IFS model cycle (CY48R1), a larger 101 member ensemble, and lower atmospheric and ocean resolutions (TCo199 with 137 vertical levels in the atmosphere, and a 1 degree version of the ocean with higher equatorial resolution and 75 vertical levels).

Vegetation is prescribed using the harmonised land forcing dataset prepared in Deliverable 1.1 (Boussetta and Balsamo 2021), that comprises of Leaf Area Index (LAI) from the Copernicus Global Land Service (CGLS) and Land Use Land Cover (LULC) from the ESA-CCI initiative.

Ocean initial conditions are provided by a low-resolution ocean reanalysis (equivalent of ORAS5), and the atmosphere is initialised from ERA5.

Two set of experiments will be performed and compared:

- Control: climatological LAI and ESA- LULC is prescribed
- Prescribed: inter-annually varying LAI and LULC is prescribed.

The land initial conditions generated using the harmonised land forcing dataset described in Boussetta and Balsamo (2021) is currently stored on tape in the ECMWF MARS archive. Due to the move of the ECMWF Data Handling System (DHS) to Bologna, the data are currently offline and the launch of the initialised hindcast experiments are on hold. With the DHS move expected to be complete only by late October, the completion of these experiments are likely to be delayed till the end of November 2022.

3.1.2 Météo-France

Following the experimental protocol, Météo-France has completed at time of writing several sets of initialised seasonal prediction experiments with 4-month forecast times, for May 1st and November 1st initial conditions. The baseline model used for the simulations is the CNRM-CM6-1 coupled climate model used for CMIP6, described in detail in Voldoire et al. (2019). This model uses lower resolution than the operational seasonal prediction system at Météo-France, with a linear truncation

at 127 spherical harmonics and 91 vertical levels in the atmospheric component, ARPEGE-Climate v6.2, and an ocean and sea ice component (NEMO v3.6 - GELATO) running on the extended e-ORCA 1° grid, with a 1/3° refinement over the equatorial band. The land-surface model, ISBA, is included in the SURFEX platform and runs at the same resolution as ARPEGE-Climate v6.2 (Decharme et al. 2019). With respect to CNRM-CM6-1, different versions of ISBA were used for the seasonal prediction experiments described in this deliverable. Three different configurations of the ISBA land-surface model are compared in the following experiments:

- Control: uses a fixed seasonal cycle of LAI corresponding to the ECOCLIMAP climatology for 1999-2005. No inter-annual variability of the vegetation is therefore accounted for in this run.
- Interactive: the ISBA-AGs version with interactive vegetation is used (as described in Deliverable 1.2, van Oorschot et al., 2022).
- Prescribed: LAI is prescribed using the harmonised LAI product designed in WP1 (Deliverable 1.1, Boussetta and Balsamo, 2021).

The CNRM-CM6 model components are initialised as follows: ocean and sea ice components are initialised from a forced NEMO-GELATO simulation constrained towards the Mercator Ocean International GLORYS2V4 reanalysis as described in Batté et al. (2020). The atmosphere is initialised from the ERA5 reanalysis (Hersbach et al., 2020), remapped to the ARPEGE-Climate grid. In-run perturbations to the ARPEGE model dynamics are introduced so as to generate 50 ensemble members, following Batté and Déqué (2016). This initialisation strategy (similar to that of the former operational system, Météo-France System 7) is used for all sets of experiments with CNRM-CM.

The land surface component is initialised by means of different offline land-surface model simulations. These are driven by ERA5, and run with the same settings as the re-forecast experiment ISBA configurations described above.

3.1.3 ISAC-CNR

The careful evaluation of the off-line simulations performed in WP1 (Deliverable D1.2, van Oorschot et al., 2022) allowed identification of the land cover/vegetation configuration that is better suited for the coupled decadal prediction experiment in WP3. The vegetation development that was decided to be used in the sensitivity experiment (hereinafter DCPP-Veg) includes the prescription of LAI from CGLS-C3S, land cover from CGLS/ESA-CCI and the consistent development of an improved parameterization of the vegetation effective cover variability (see van Oorschot et al., 2022 for details).

The improved vegetation variability from WP1 has been implemented in the EC-Earth3 coupled model for the DCPP-Veg experiment to cover a subset of the tier-1 (Component A1) decadal hindcasts already performed at BSC for the Decadal Climate Prediction Project (hereinafter DCPP-Ctr; Bilbao et al., 2021). The resulting set of improved decadal hindcasts (5-year; 10 members) starts November 1st of each year in the period 1993-2014, following availability of the latest generation satellite-derived land cover and vegetation observations (Boussetta and Balsamo, 2021). DCPP-Ctr and DCPP-Veg share the same configuration, resolution and initial conditions but the land surface.

To initialise the land for DCPP-Veg, separate ERA-Land off-line simulations have been performed with the ERA5 atmospheric forcing (Hersbach et al., 2020). This was needed to ensure in DCPP-Veg the equilibrium between the initialised land states with the atmosphere to avoid any possibility of artificial drifts that could affect the comparison.

In collaboration with the colleagues at Barcelona Supercomputing Centre (BSC), the Autosubmit workflow manager (https://autosubmit.readthedocs.io/en/v3.13.0/) has been employed to set-up a semi-automated procedure for the production of the DCPP-Veg retrospective forecasts. To this aim the EC-Earth runtime scripts have been modified in order to perform parallel scheduling of the decadal predictions and post-processing and by setting up the required running environment including preparation and transfer in the working directory of the initial and boundary conditions required by the model. At the time of writing, we have completed a first set of 5 start dates and we are currently analysing the outputs before continuing with the full set of hindcasts.

3.1.4 Additional experiments

As a collaborative effort with ECMWF, ISAC-CNR included a parameterization of the effective vegetation-cover variability in the ECMWF SEAS5 (low resolution version) to evaluate the effect on the seasonal forecasts starting 1st of November. The parameterization is suitably obtained from what was previously tested and developed in the framework of EC-Earth (Alessandri et al., 2017; Döscher et al., 2022).

The experiments described in this section are not included in the experimental protocol. Results of their analysis are reported here as they are tightly linked to scientific questions within WP3. We use version 5 of ECMWF seasonal prediction system (SEAS5; Johnson et al 2019) at low-resolution configuration (Tco199 atmosphere, ORCA1L75 ocean; hereinafter lowres). Two 25-member ensembles of retrospective predictions are performed using (i) standard (CTRL) and (ii) modified (SENS) versions of the SEAS5 lowres for the period 1982-2014 (1st November start dates). The same configuration, resolution and initial conditions of SEAS5-lowres have been used in both CTRL and SENS, except for land surface. The difference over land is that the SENS version allows vegetation fractional coverage to change as a function of Leaf Area Index (LAI) for both low and high vegetation following the approach described in Alessandri et al. (2017). To initialise land, two distinguished ERA-Land off-line simulations have been performed with the same atmospheric forcing (ERA-Interim; Dee et al. 2011) and configuration but the effective vegetation-cover implementation in SENS. This is needed to make sure the initialised SENS is also in equilibrium with land initial conditions to avoid any possibility of artificial drifts that could affect the comparison. For SENS, both off-line simulation and hindcasts have been driven with observed LAI from 1982-2014 LAI3g data (Zhu et al., 2013).

The satellite observations of surface albedo (GLASS-GLCF; Liu et al., 2013) are used for the verification; ERA5 reanalysis (Hersbach et al. 2020) is the reference dataset for all the other surface climate variables considered in the evaluation (2m Temperature; Mean Sea Level pressure, snow depth, and surface fluxes of sensible and latent heat).

3.2 Preliminary results

This section shows preliminary results assessing the influence of improved land surface on seasonal prediction quality.

3.2.1 Seasonal prediction of LAI

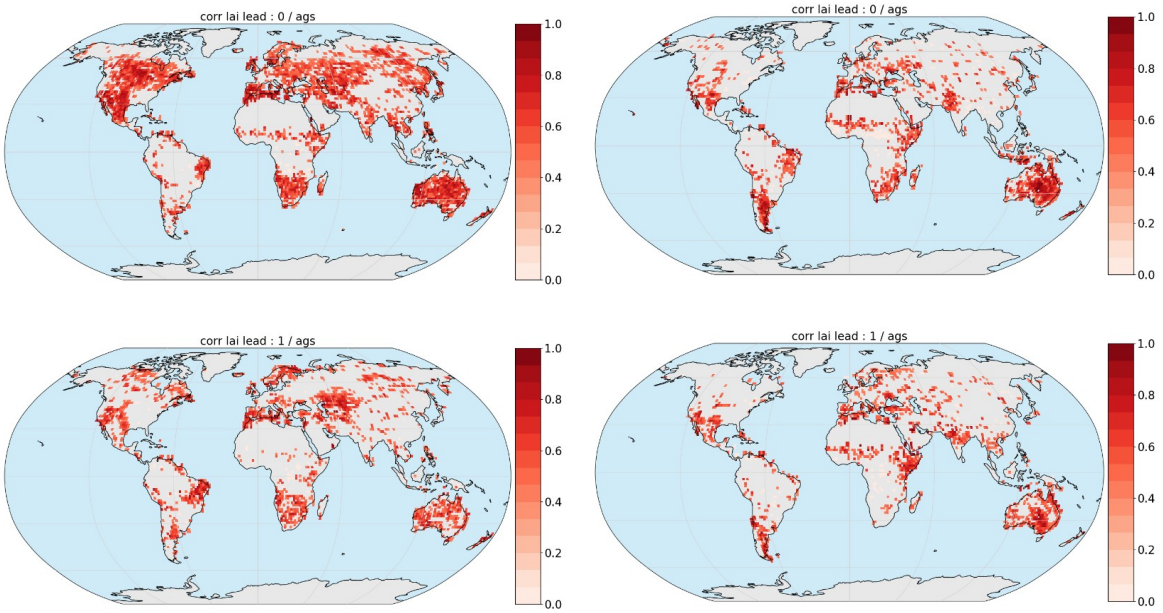

Figure 1: Inter-annual correlation between LAI harmonised data (Boussetta and Balsamo, 2021) and forecast LAI in the Interactive re-forecasts (with the interactive vegetation scheme) for the forecast month 0 (top row - May on the left and November on the right) and for the first trimester (bottom row - JJA on the left and DJF on the right) for 1993-2016. Non significant correlations (at the 95% level according to a Student t-test) are not shown.

A first focus of the analysis of Météo-France experiments with CNRM-CM was set on the evaluation of the forecast quality of the Interactive re-forecasts (which include interactive vegetation) for LAI. Figure 1 shows the correlation of LAI with the reference harmonised dataset from WP1 in these re-forecasts for the May initialisation (left column) and November initialisation (right column) at forecast month 0 (top row) and the first season (bottom row, JJA and DJF, respectively). Some areas with significant skill are found, but skill even during the first month after initialisation is restricted to some areas of the globe (South Africa, Australia, mid-latitude regions) and drops sharply for both initialisation dates studied. The skill is generally higher for boreal summer than austral summer. Unlike atmospheric variables, skill is typically lower in the tropical band than over midlatitudes. This may be due to the lower interannual variability of LAI relative to a high mean state over the tropics.

Reasons for this modest skill (especially during the first month where some persistence of the signal is expected for LAI) were investigated by comparing the LAI from the offline simulations (SURFEX driven by ERA5) used to initialise the Interactive re-forecasts with the reference dataset from D1.1. Figure 2 shows the correlation for DJF (left) and JJA (right). It represents an estimate of the upper boundary of skill that could be expected from the seasonal forecast of LAI with this model configuration. The low correlation over some areas could result from known limitations in the interactive vegetation scheme in the ISBA model, discussed in deliverable D1.3.

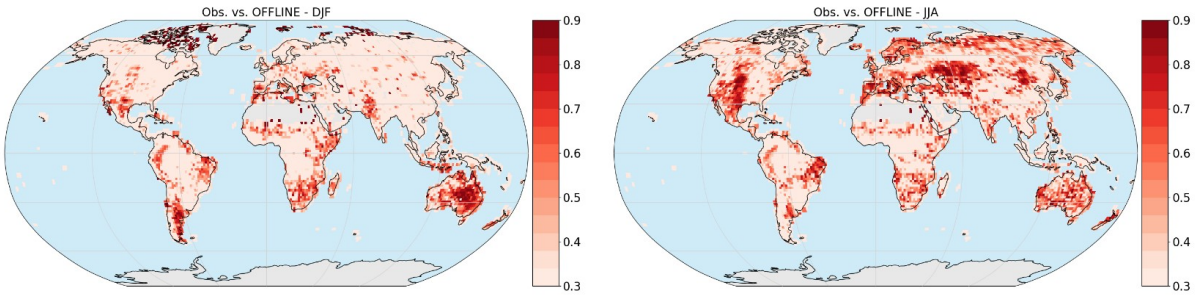

Figure 2: Inter-annual correlation between the observations of LAI from D1.1 and LAI simulated by Surfex in the offline run with the interactive vegetation scheme used to initialise the Interactive re-forecast set. Results are shown for DJF (left) and JJA (right) for the period 1993-2019.

A preliminary conclusion from this work is that a substantial part of the limitations found in the LAI correlation levels in seasonal re-forecasts with interactive vegetation arise from the limitations of the interactive vegetation model itself in representing observed interannual variability. Similar results were found (not shown) by comparing these simulations to another observational dataset for LAI. The seasonal forecast system setting with the interactive vegetation is already quite close to the estimate of its maximum predictability. One implication of this result is that improvements in the vegetation model could translate into a direct improvement of the seasonal forecast of LAI in the tropics, or even in the mid-latitudes (even if more limited).

3.2.2 Impact of interactive vegetation on surface variables forecasts

A next step in the evaluation of the influence of interactive vegetation in the Météo-France re-forecasts was to assess the impact of these settings on the seasonal forecast skill of other variables (atmospheric variables and land surface fluxes). To this end, the set of Interactive re-forecasts is compared in terms of skill with Control.

The left column of Figure 3 shows (where significant) the near-surface temperature (TAS) correlation with ERA5 in the first season following initialisation (JJA for May starts, DJF for November starts), for the Interactive re-forecasts. On the right column, differences with the correlation obtained with the Control re-forecast, which uses the ECOCLIMAP climatology, is shown. Significant differences are hatched. Many regions exhibit limited skill for TAS, consistent with previous evaluations of the CNRM-CM6-1 model in seasonal prediction mode. As expected, skill is higher over the Tropics than mid- and high-latitudes. In terms of improvement or degradation with respect to the Control re-forecast, regions with significant differences in correlation are scarce. Some degradation of skill is found for JJA over Southern and Central Europe, whereas improvements are found for the British Isles. However, the skill in these areas is very low so consequences of these improvements and degradations are limited. For DJF, regions where skill is improved are arguably larger, but overall differences are very small.

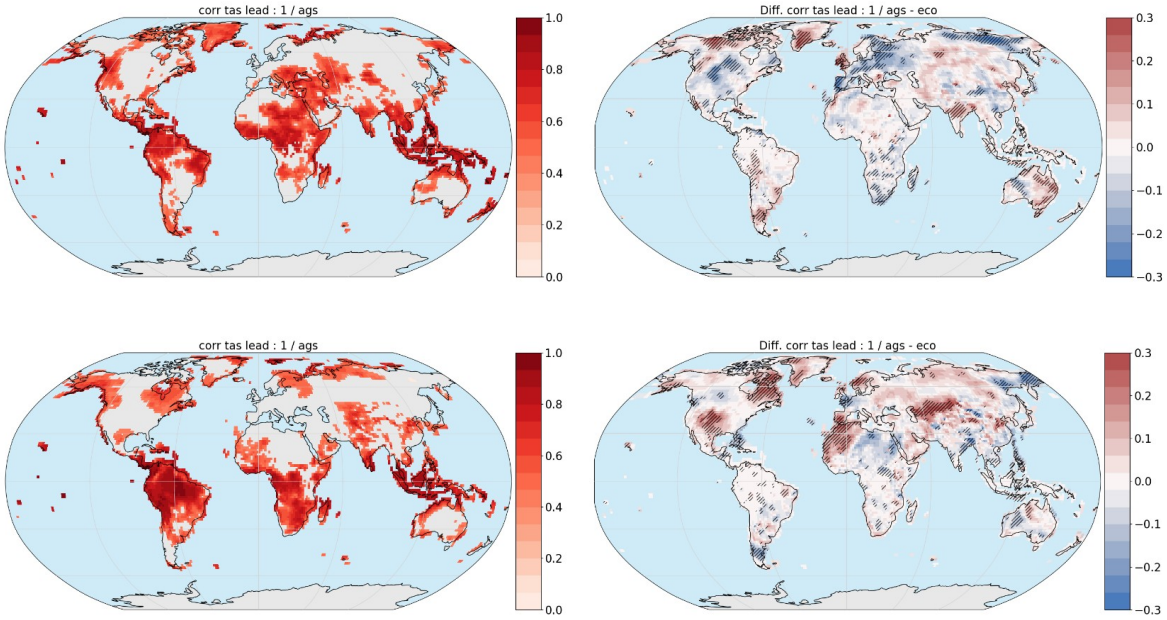

Figure 3: (Left) Inter-annual correlation between ERA5 near-surface temperature and forecast near-surface temperature with the interactive vegetation scheme (Interactive) for the first forecast trimester. (Right) Inter-annual correlation differences of forecast near-surface temperature with respect to ERA5 (Interactive - Control) in the Interactive re-forecasts (with the interactive vegetation scheme) and the Control (using ECOCLIMAP climatology) for the first forecast trimester. The top row is for JJA, initialisation in May; bottom row is DJF, initialisation in November, and the re-forecast period is 1993-2016.

In order to further assess the influence of the interactive vegetation on seasonal re-forecasts, skill of surface - atmosphere fluxes was also assessed. Figure 4 shows results for the surface latent heat flux evaluated against the DOLCE v3 dataset (Hobeichi et al., 2021). The skill in the Interactive re-forecasts is more patchy than for near-surface temperature, with the exception of South Africa, Northeast Brazil and Australia for austral winter (JJA) and the Sahel region in boreal winter (DJF). Changes with respect to the Control re-forecasts are very limited.

These correlation assessments are quite preliminary at this stage, and call for further analysis. One first question tackled was the potential predictability of LAI in a perfect model framework (not shown), which demonstrated that LAI does have some persistence in the CNRM-CM model predicting itself. Substantially higher levels of skill are found in this perfect model framework, although skill does drop with forecast time. This indicates that the weak improvements and even degradation found may result from model limitations, and that introducing an interactive vegetation scheme in the CNRM model will not significantly alter seasonal prediction results (but on the other hand, won't significantly improve these either, despite additional computational costs).

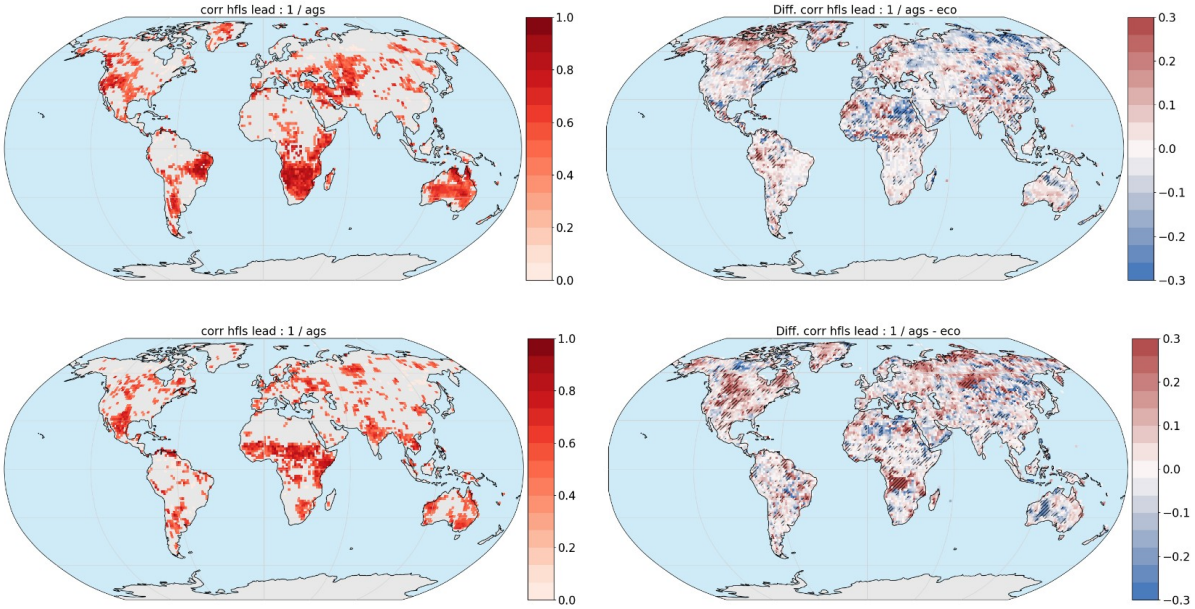

Figure 4: Same as Fig. 3 for the latent heat flux. The reference here is DOLCE v3.

3.2.3 Influence of a realistic effective vegetation-cover on SEAS5 seasonal re-forecasts

Results from the additional experiments described in section 3.1.4 are presented here.

Figure 5a) shows the difference of the correlations with observed 2m-temperature between SENS (i.e. the new version in which the effective vegetation-cover variability is parametrised) and CTRL (the standard SEAS5 configuration) in the ensemble-mean seasonal forecasts at 1-month lead-time for the 2-4 month forecast period valid in DJF. For each grid point, we tested the null hypothesis of whether correlation differences occurred simply by chance through a Monte Carlo bootstrap method (1000 repetitions). Overall, the performance of SENS is better than CTRL, especially in the Northern Hemisphere. The SENS experiment displays increased correlations over Siberia and further west matching the distribution of Euro-Asian Boreal forests, and also in Greenland.

To investigate the coupling and the possible predictability sources, the relationships between the improvement of the correlation for the target variable (e.g. 2 m-temperature) is analysed with respect to the improvements in the possible surface drivers for the areas of interest (e.g. surface snow depth, surface albedo, soil moisture). For this purpose, the correlation coefficient is decomposed in its components measuring the covariance between each predicted (x) and observed (y) yearly (i) anomalies [hereinafter normalised yearly covariance, $r(x,y)_i$] following the approach in Alessandri et al (2017). The SENS minus CTRL difference in the normalised yearly covariance [$\Delta r(x,y)_i$] is analysed to identify the possible surface contributor to the enhanced predictability of the target variables due to the improved land surface conditions. To this aim, the linear relation between the target and driver fields is assessed using a least square method, and the significance of the slope of linear relationship is evaluated using a Fisher parametric test. The positive linear relationship between target and driver in terms of the SENS-minus-CTRL indicates the change of predictability of the target as mediated by the driver, which is directly affected by the difference in the land surface. Only the linear coefficients of the regression that passed the significance test at a 10 % level are

considered. The analysis reveals a strong local coupling of the improved skill in 2m temperature, over Euro-Asian boreal forest coming from the surface albedo (Figure 5b). In fact, SENS displays a significant improvement in surface albedo compared with CTRL over Siberia (Not shown). Interestingly, the orange years (indicating when both target and driver lie in the lower/upper terciles of their respective distribution) on the upper-right quadrant of Figure 5b indicate that the positive effect of the surface-albedo coupling occurs in years of strong NAO activity (except for 2005). On the other hand, the orange years on the lower-left quadrant of Figure 5b occur in relatively neutral NAO years. This result suggests that the coupling from the land surface albedo might operate by amplifying the signal originating from the North Atlantic sector therefore producing improved T2m skill locally when the NAO teleconnection is active.

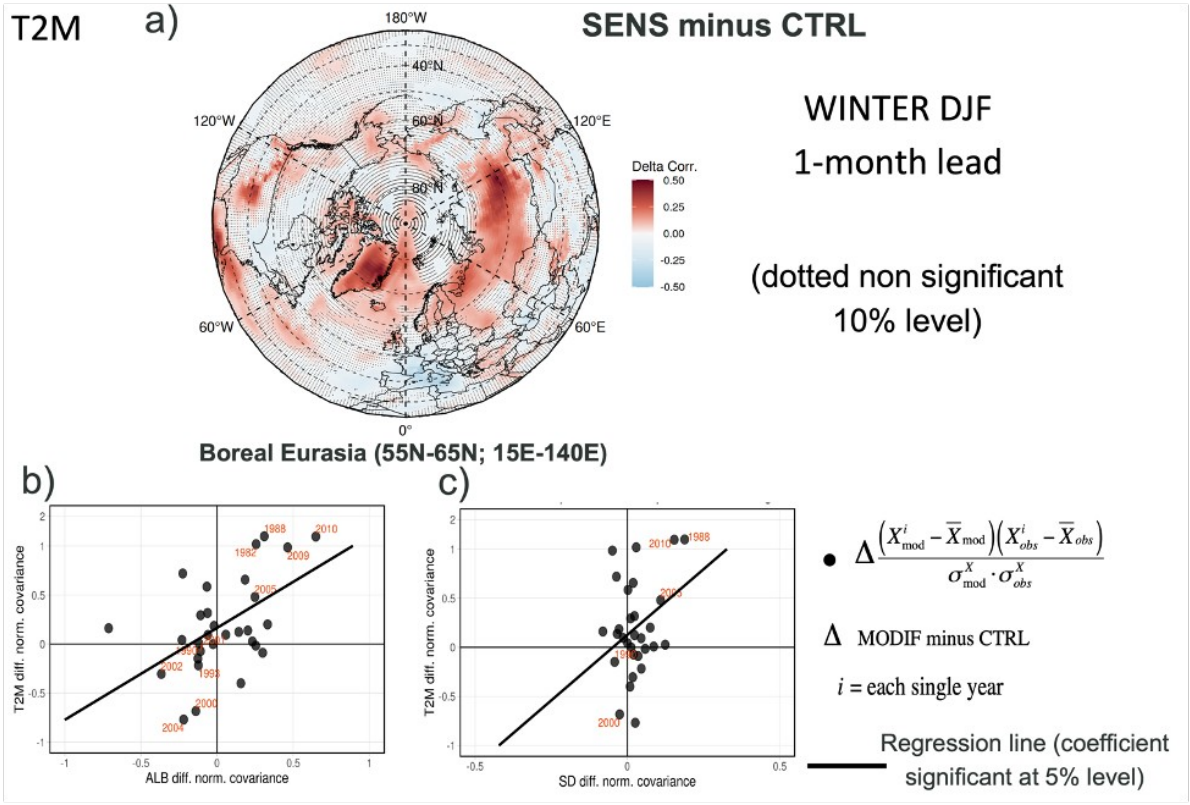

Figure 5:a) 1-month-lead boreal winter (DJF) 2 m temperature SENS minus CTRL correlation difference vs. ERA-5. Dotted grid points did not pass a significance test at 10 % level. b,c) Scatterplot of the normalised yearly covariance differences between SENS and CTRL [$\Delta r(x,y)ki$] for the predictions averaged over the Eurasia boreal forest domain (15E–140E; 55N–65N) of b) T2m versus albedo and c) T2m versus snow-depth. Black filled circles are the normalised yearly covariance differences for each start date (i = 1, 2, ...,33). Regression line indicates significant (10 % level) relationship between improved prediction of T2m and enhanced b) albedo and c) snow depth. Orange years indicate when normalised yearly covariance differences change in the same direction (i.e. both target and driver lying in the lower/upper terciles of their respective distribution).

From the regions with the largest 2m temperature improvements over Siberia, a large-scale circulation response originates encompassing Northern Hemisphere mid-to-high latitudes from Siberia to the North Atlantic, as demonstrated from the ACC difference in mean sea level pressure (MSLP; not shown). It corresponds to a significant MSLP ACC-enhancement over Siberia that extends further towards the northwest, also affecting, to some extent, the North Atlantic and Arctic domains. The leading mode (EOF1) of DJF MSLP interannual variability over the North Atlantic sector [20N-

80N; 90W-40E] appears to be slightly better represented in SENS compared to CTRL (not shown). Importantly, the correlation between the NAO index computed from the corresponding first Principal Component (PC1) against ERA5 shows a significant improvement in SENS. In fact, the correlation coefficient increases from 0.18 (not statistically significant at 5% significance level) in CTRL to 0.34 (statistically significant 5% significance level) in SENS (see Table 1).

*Table 1: Correlation between the predicted NAO index [computed as the PC1 of leading mode (EOF1) of DJF MSLP interannual variability over North Atlantic sector; 20N-80N; 90W-40E] for SENS (1st row) and CTRL (2nd row) experiments against ERA5. ** indicates statistically significant correlation at the 5% level.*

Correlation vs. ERA5	NAO
SENS	0.34 **
CTRL	0.18

The outcomes of this analysis will be further discussed in a peer-reviewed paper for the scientific community that is currently in preparation (Alessandri et al., in prep.).

4 Impact of aerosols on initialised predictions

4.1 Progress on initialised prediction experiments

4.1.1 ECMWF

Following the experimental protocol (Deliverable D3.1), sets of 13-month initialised hindcast experiments initialised 1 November and covering the historical period 1981-2020 are being performed using the seasonal configuration of the ECMWF IFS coupled model (see section 3.1.1). These experiments include:

- OLDTROP: Standard Control experiment with current operational aerosol climatology and volcanic aerosols
- NEWTROP: Experiment with newly developed smoothly time varying aerosol climatology as part of D2.1.
- FIXTROP: Experiment with recent-period CAMS aerosol climatology

The standard Control experiment OLDTROP has been completed and the NEWTROP and FIXTROP experiments will be launched imminently. At time of writing, these experiments are expected to be completed to meet milestone M3.2 set for M24.

The WP3 integrations to assess the impact of improved volcanic aerosol on seasonal predictions have not yet started, due to WP2 delays in setting up and testing the improved aerosol treatment. Work on the set-up on the new Atos computers is ongoing, and it is planned that the low-resolution 13 month experiments will be run first, followed by the high resolution runs. At time of writing, the low-resolution runs are expected to be completed by December, and the high resolution runs by the end of January.

4.1.2 BSC

The Decadal Climate Prediction Project (DCPP, Boer et al, 2016) jointly with VolMIP (Zanchettin et al, 2016) defined a set of coordinated experiments seeking to understand the effects of volcanoes on past and potentially on future decadal predictions. The DCPP component A consists of 10-member ensembles of 10-year-long predictions initialised from observations every year from 1960 to 2018 and including CMIP6 historical values of atmospheric composition and/or emissions. With the objective of determining the impact of the major volcanic eruptions that occurred during this period (Mount Agung, 1963; El Chichón, 1982; and Mount Pinatubo, 1991), the complementary DCPP component C protocol consists in repeating hindcasts initialised shortly before the eruptions of Mount Agung (1963), El Chichón (1982) and Mount Pinatubo (1991) and replacing the volcanic forcing by the “background” volcanic aerosol (i.e. its mean over the period 1850-2014). Hence we analyse two sets of the prediction ensembles for the 1962, 1981 and 1990 start dates. The impact of the volcanic eruptions is therefore determined by subtracting the hindcasts with and without the volcanic aerosols (DCPP-A - DCPP-C). We take advantage that five other prediction centres, as well as BSC, have performed these CMIP6 simulations (CanESM5, CESM1, EC-Earth3, HadGEM3, IPSL-CM6

and CMCC) and we carry out a multi-model analysis of the impact of volcanic eruptions on decadal predictions (Bilbao et al., in prep.).

In a separate exercise we have performed experiments to evaluate the adequacy of different available modules to estimate the distribution of sulphate aerosols generated by a given eruption. This is motivated by the fact that in real-time prediction, should a new major volcanic eruption occur, its effects on the climate and predictability could only be reproduced with a good estimate of its associated stratospheric sulphate aerosol evolution. For this purpose modules such as the Easy Volcanic Aerosol (EVA, Toohey et al., 2016) and it's more recent version Easy Volcanic Aerosol Height (EVA_H, Aubry et al., 2020), can be used to generate the stratospheric aerosol forcing due to a volcanic eruption which then can be used as input in climate models. In WP2 the necessary developments have been carried out to perform decadal climate predictions with stratospheric aerosol forcings generated with EVA_H. To evaluate the climate response to volcanic forcings generated with EVA_H, we will repeat the hindcasts initialised in 1962, 1981 and 1990 (as in DCPP-C), but with the volcanic forcings estimated with EVA_H (DCPP-C-Agung_EVA-H, DCPP-C-ElChichon_EVA-H and DCPP-C-Pinatubo_EVA-H). Comparing these simulations to DCPP-A and C will allow us to compare the climatic impacts of the volcanic forcings estimated with EVA_H and will indicate the expected uncertainty in the climate response when used operationally in the case of a future volcanic eruption. The DCPP-C-Pinatubo_EVA-H experiment has been completed and we show preliminary results in section 4.2.2.

4.2 Preliminary results

This section reports results on the impact of volcanic aerosols based on experiments described in the previous paragraphs.

4.2.1 Impact of volcanic eruptions in CMIP6 decadal prediction systems: a multi-model analysis

Explosive volcanic eruptions have climate impacts on seasonal-to-decadal time-scales which have high predictive potential (e.g. Ménégoz et al., 2018; Hermanson et al., 2020; Marshall et al., 2022). In recent decades three major volcanic eruptions have occurred whose effects are included in decadal prediction hindcasts: Mount Agung (Mar-Sept 1963), El Chichón (Feb-Mar 1982) and Mount Pinatubo (Jun 1991). This coordinated multi-model analysis seeks to determine the climate signals that were caused by them by using the DCPP predictions. We use results from six state-of-the-art decadal prediction systems from CMIP6: CanESM5, CESM1, EC-Earth3, HadGEM3, IPSL-CM6 and CMCC. Each prediction system has 10 ensemble members of 10 forecast years with and without the volcanic forcing for each of the three volcanic eruptions, making a total of 180 members.

Following the volcanic eruptions, the global mean surface temperature drops in response to the negative radiative forcing, and recovers after approximately 5-7 years (Fig. 6). As expected, the surface temperature response varies with the magnitude of the eruption. The response among models is comparable and consistent with previous studies (e.g. Hermanson et al., 2020).

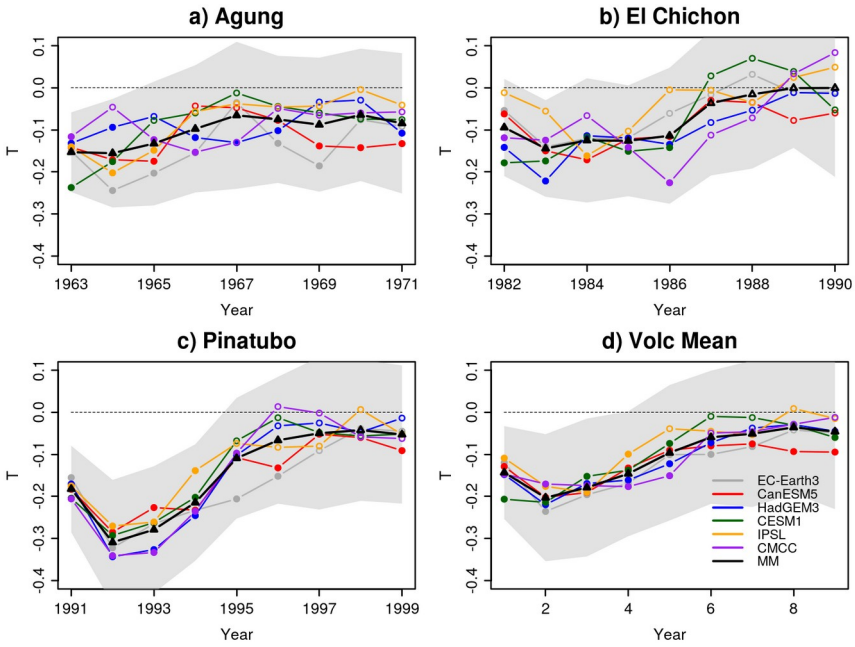

Figure 6: Global annual mean surface temperature (ºC) response (dcppA-dcppC) to the eruption of a) Mount Agung (1963), b) El Chichón (1982), c) Mount Pinatubo (1991) and d) the mean of the three eruptions. Filled dots indicate statistically significant differences between the hindcasts with and without the volcanic forcing. The shading is the multi-model member spread computed as ± one standard deviation from the multi-model ensemble mean.

The surface temperature response in the first year following the volcanic eruptions shows a distinct pattern, characterised by a generalised cooling, which is largest in the Tropics, and a warming in the Eurasian Arctic sector (Fig. 7a-d). For forecast years 2-5, the cooling is worldwide and the Arctic shows largest anomalies (Fig. 7e-h). The patterns are consistent across all the models and for the individual volcanic eruptions. At later forecast times (years 6-9) the temperature anomalies decrease, consistent with the recovery following the eruption, and differences among the models and eruptions emerge.

The warming in north Eurasia has been linked to changes in the atmospheric circulation in response to volcanic forcing (e.g. Driscoll et al., 2012). This dynamical response may be explained by an acceleration of the polar vortex due to warming of the stratosphere, which projects onto a positive phase of the NAM or NAO (Fig. 8). Our analysis, however, shows that the warming already starts developing in the first JJA, before a response in the Polar atmospheric circulation is evident. We are currently exploring the causes of that early warming.

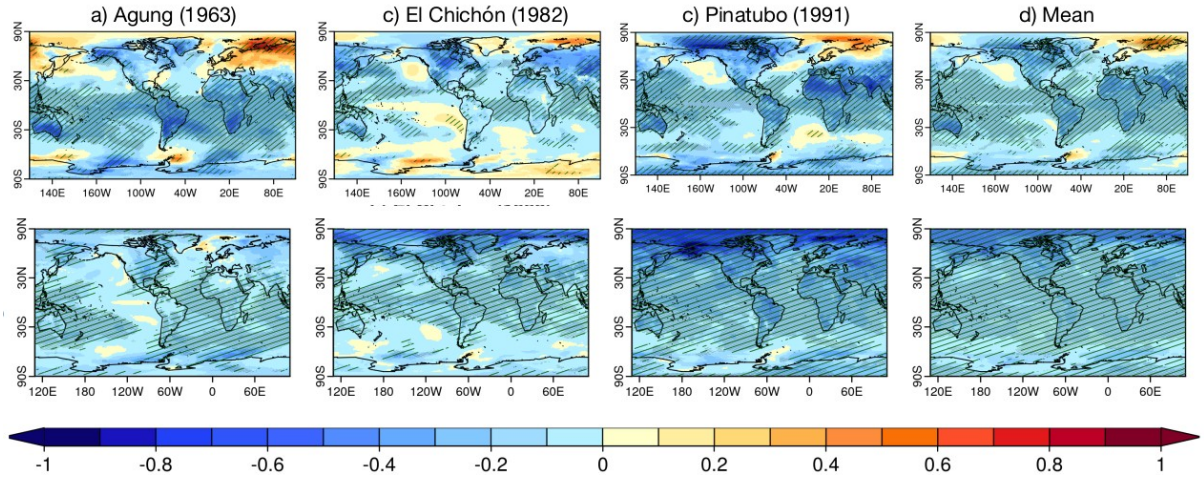

Figure 7: Multi-model mean surface temperature (ºC) response (dcppA-dcppC) the first year (June-May) following the eruptions of a) Mount Agung (1963), b) El Chichón (1982), c) Mount Pinatubo (1991) and d) the mean of the three volcanoes, and for forecast years 2-5 (e-h). Hatching indicates statistically significant anomalies and shading indicates model sign consistency.

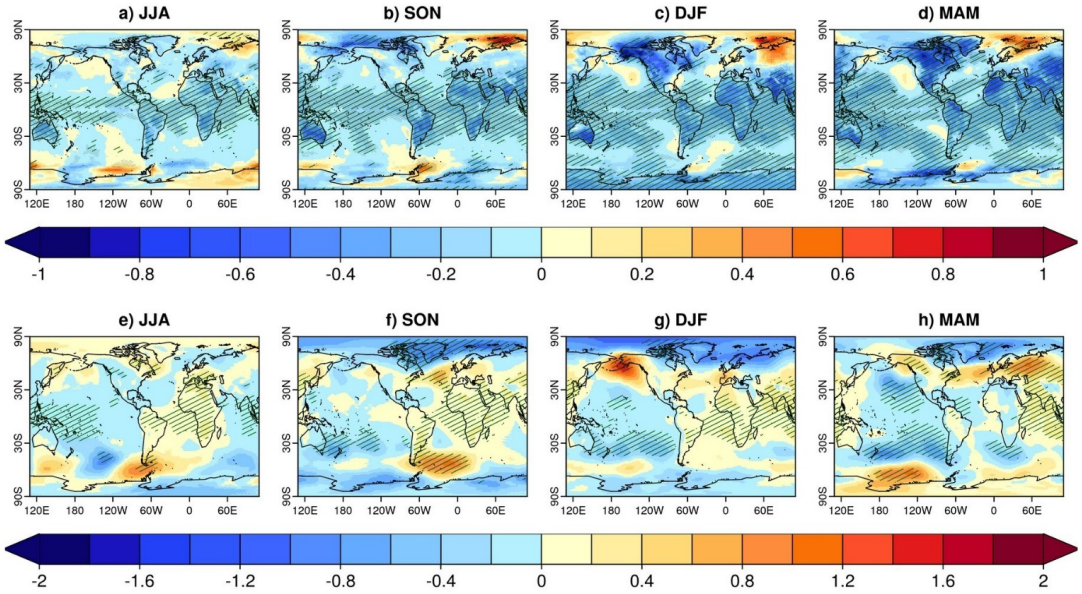

Figure 8: Surface air temperature (a-d) and sea level pressure (e-h) for each season the first year following the volcanic eruptions. Hatching indicates statistically significant anomalies and shading indicates model sign consistency.

Previous studies have shown that volcanic eruptions impact the El Niño Southern Oscillation (e.g. Khodri et al., 2017). The multi-model mean shows that an El Niño response develops following the eruptions, which peaks on the second DJF (Fig. 9). The response is strongest for Agung and Pinatubo and less so for El Chichón. For the 1991 Pinatubo eruption a La Niña follows peaking on the third DJF, but this is not evident for the other two eruptions. The differences in the response for each eruption may be explained by the differences in eruption magnitude and/or background state when the eruption occurs.

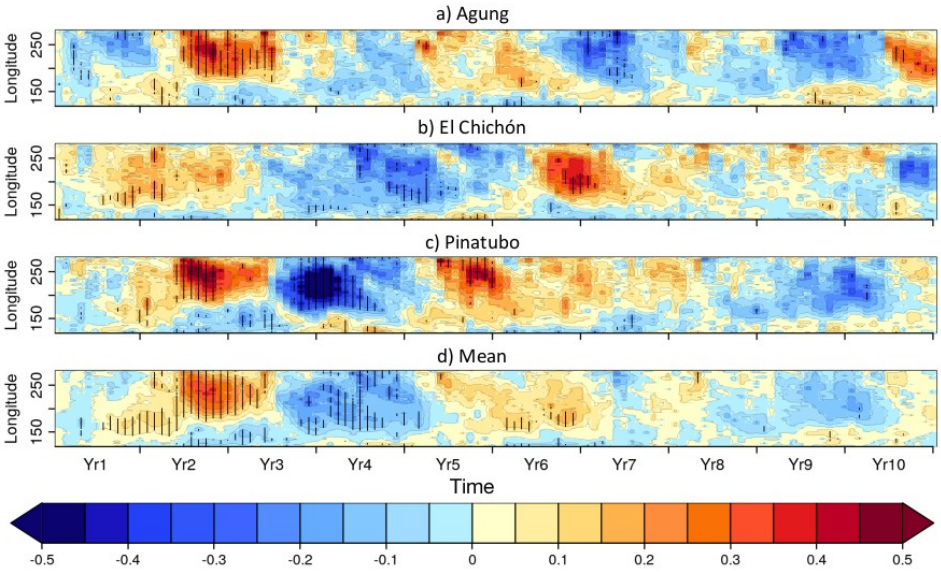

Figure 9: Model mean relative tropical SST (5N-5S) response (after subtracting the mean from 60N-60S) following the eruptions of a) Mount Agung (1963), b) El Chichón (1982), c) Mount Pinatubo (1991) and d) the mean of the three volcanoes. Stippling indicates statistically significant anomalies.

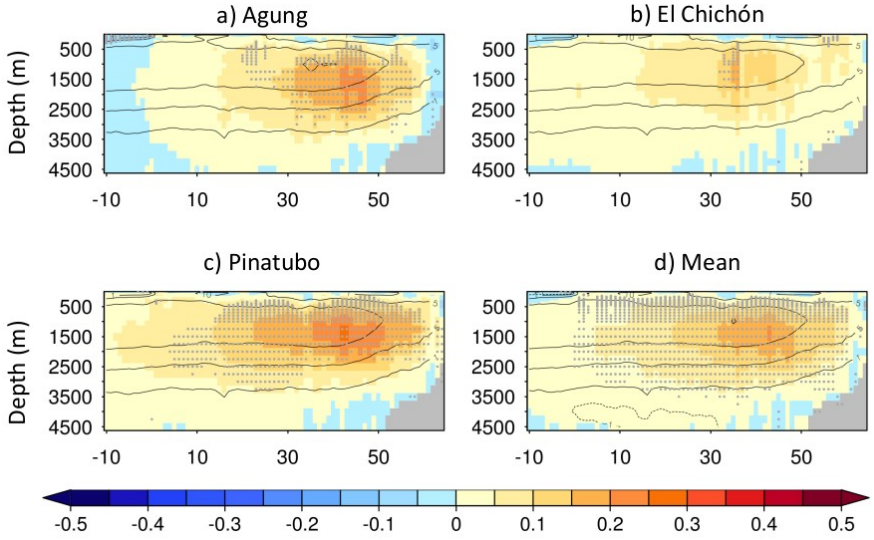

Figure 10: Model mean response of the overturning stream function (Sv) to the volcanic eruptions. Contours show the overturning stream function in the DCPP-C predictions. Stippling indicates statistically significant anomalies.

The North Atlantic Ocean is a region where recent volcanic eruptions have been shown to induce changes on decadal timescales (e.g. Swingedouw et al., 2017). The multi-model mean response shows an increase in the mixed layer depth the three winters following the eruption (not shown) and a strengthening of the AMOC in years 2-9 (Fig. 10), but the results are largely model dependent, with HadGEM3, CMCC and CESM1 showing a significant response while the rest do not.

These results highlight the strong climate effects of large volcanic eruptions, ranging from months to decades, which can be important at the local scale, and thus substantially degrade the skill of the predictions when a new major volcanic eruption occurs. Hence it is important to develop methods to

quickly generate the volcanic forcing associated with such eruptions, so that new predictions can be produced soon after their occurrence.

4.2.2 Preliminary results of the climate response to the EVA and EVA_H volcanic forcings in EC-Earth3

We have recently completed the hindcast for the 1990 Pinatubo eruption for both EVA and EVA_H, for which preliminary results are described next.

To compare the radiative response to the Pinatubo idealised (EVA_H and EVA) volcanic forcings with CMIP6, we first look at the global mean top-of-atmosphere radiation (TOA) balance (Fig. 11a), calculated as anomalies of incoming shortwave minus outgoing shortwave and out-going longwave radiation. The TOA radiative flux anomalies show that in the first year following the Pinatubo eruption (largest negative anomaly) the impact of the EVA_H forcing on the net incoming energy is approximately 40% weaker than for the CMIP6 forcing, while EVA forcing is approximately 10% stronger (Fig. 11a). The TOA radiative flux anomalies also recover faster with the EVA forcing. These results are consistent with forcing differences found in WP2.

The global mean surface temperature response (Fig. 11b) shows a progressive post eruption cooling until approximately 1993, when the cooling reaches its maximum with all three forcings. Consistent with the TOA radiative flux differences, even if the differences in both variables do not relate linearly, the EVA_H forcing yields weaker negative global surface temperature anomalies (~-0.3℃) than CMIP6 (~-0.4℃), while EVA forced anomalies remain close to the CMIP6 forced ones. Although the CMIP6 and EVA temperature response is similar this is for the wrong reasons as the EVA forcing is initially stronger (consistent with greater negative temperature anomalies early on) and persists for a shorter time, while CMIP6 is weaker but lasts for longer.

The global mean temperature in the lower stratosphere (50 hPa) shows strong post eruption warming anomalies, with small ensemble spread in comparison to other variables, and clearly illustrates fundamental differences induced by the forcings (Fig. 11c). Consistent with the results described previously, the EVA_H forcing produces a weak response (~1.5℃) in comparison to CMIP6 forcing (~2.8℃), while with the EVA forcing the response is stronger (~3.6℃). There are evident temporal structural differences in the nature of the response to the idealised forcings, with the EVA_H and CMIP6 signals showing qualitative similarities (despite the difference in magnitude), while EVA signal peaks sooner and recovers faster. The differences in the stratospheric temperature response may particularly impact the atmospheric dynamical response, such as the Eurasian warming (e.g. DallaSanta and Polvani, 2022).

The induced upper ocean heat content changes also reveal differences for the three forcings (Fig. 11d). It is particularly evident that the upper ocean heat content decrease persists much longer for the CMIP6 forcing, while both EVA and EVA_H show a decrease and faster recovery, as indicated by the anomalies not being statistically significant after 5-6 years. Again, the temporal structure in response to EVA_H resembles that of CMIP6 but scaled down.

These preliminary results highlight the limitations of the simple aerosol forcing generator models to produce realistic volcanic forcings, with considerable errors, both quantitative and qualitative, as revealed by the global mean averages. The next steps in the analysis will focus on comparing the

geographical and vertical differences once the rest of hindcasts experiments for the Agung and El Chichón eruptions have been performed.

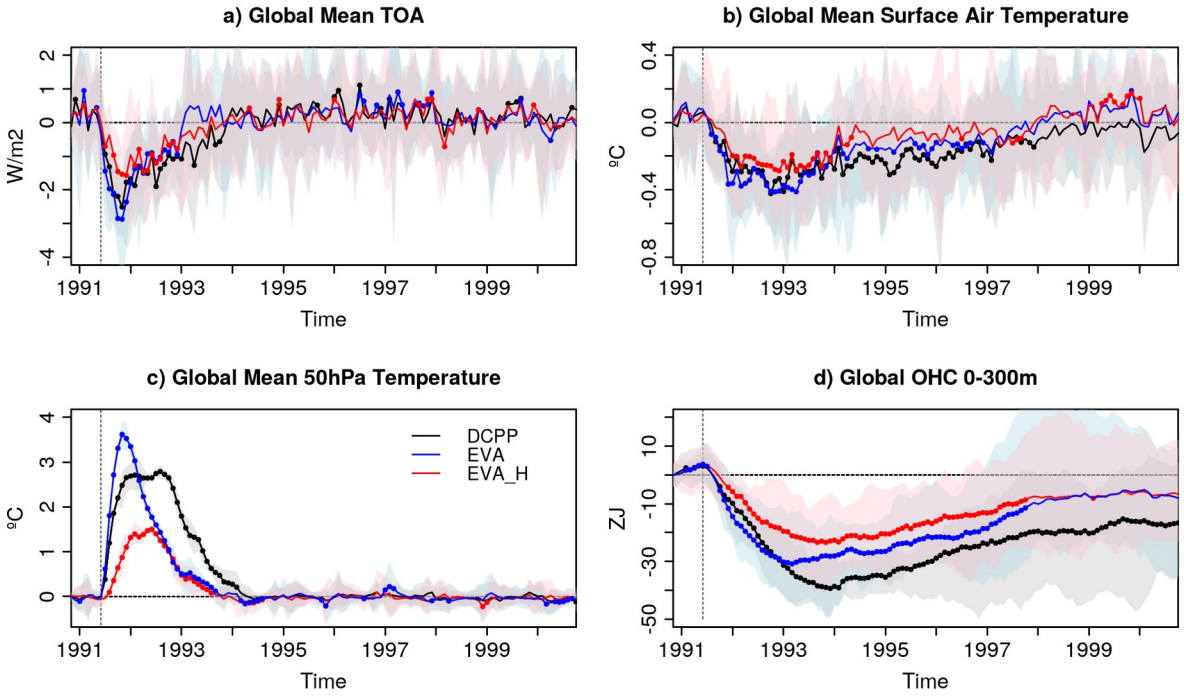

Figure 11: a) Global mean a) top-of-atmosphere radiation, b) surface temperature, c) 50hPa temperature and d) ocean heat content in the upper 300m for the hindcast set initialised in November 1990 and forced with CMIP6, EVA and EVA_H volcanic forcings. Dots indicate statistically significant differences ($p < 0.05$) according to two-sided T-test.

5 Future plans

The results presented in this deliverable are intermediate results, to be completed with the analysis of experiments still underway at time of writing. Main plans for the final year of the project include the following:

- Further analysis of results with the Météo-France re-forecasts with different land surface configurations to clarify the influence of time-evolving and interactive vegetation on predictability over the tropics and mid-latitudes;
- Completion and analysis of the ECMWF experiments planned for task 3.1 (influence of land surface);
- Analysis of results on the influence of time-evolving land use / land cover boundary conditions in a multi-model framework;
- Focus on specific case studies (drought, heat waves) and analysis of influence on extremes;
- Completion and analysis of the ECMWF experiments planned for task 3.2 (influence of tropospheric aerosols and volcanic aerosols on seasonal prediction quality);
- Completion of the ISAC-CNR decadal re-forecasts (DCPP-Veg) with EC-Earth including prescribed LAI and improved effective cover vegetation variability, and analysis of results;
- Completion of the remaining BSC EVA_H and EVA decadal re-forecasts and analysis of results;
- Comparison of results with volcanic aerosols in initialised re-forecasts from BSC and ECMWF.

These lines of work will contribute to the forthcoming deliverables D3.2 and D3.3 due at the end of the project.

6 Conclusion

This deliverable presents an overview of the status of ongoing work in CONFESS work package 3. Most results described in this document are preliminary, and further analysis is in progress.

Some intermediate conclusions have been reached in view of results presented here:

- Improvements in the realism of the representation of the leaf area index can influence re-forecast quality: experiments with a refined vegetation are compared to SEAS5 and show increase in near-surface temperature skill in the Northern Hemisphere during boreal winter, and further analysis suggests this is due to improvements in the surface albedo which translates into better prediction of mean sea level pressure anomalies.
- Implementing an interactive vegetation scheme in a coupled system does not necessarily improve near-surface temperature skill despite enhanced physical consistency of surface fluxes.
- Large volcanic eruptions have a strong influence on climate anomalies at the multi-annual time scale, particularly over the North Atlantic sector. Based on preliminary results for the Pinatubo eruption, the EVA_H idealised forcings have a lower impact on these anomalies than the CMIP6 forcings and might underestimate the effect of new volcanic eruptions.

These conclusions will be consolidated through further analysis, and, when relevant, a multi-system assessment.

7 References

CONFESS deliverables

Boussetta, S. and Balsamo, G. (2021). CONFESS D1.1: Vegetation dataset of Land Use/Land Cover and Leaf Area Index.

van Oorschot, F. et al. (2022). CONFESS D1.2: Improved vegetation variability.

Stockdale, T., Senan, R. and Bilbao, R. (2022). CONFESS D2.2: Harmonized CAMS and CMIP6 datasets for aerosols.

Batté, L. and Stockdale, T. (2021). CONFESS D3.1: Experimental protocol for land and aerosol forcing re-forecasts.

Peer-reviewed articles

Alessandri, A., Catalano, F., De Felice, M. et al. (2017). Multi-scale enhancement of climate prediction over land by increasing the model sensitivity to vegetation variability in EC-Earth. Clim. Dyn. 49: 1215–1237. https://doi.org/10.1007/s00382-016-3372-4

Aubry, T. J., Toohey, M., Marshall, L., Schmidt, A., and Jellinek, A. M. (2020). A new volcanic stratospheric sulfate aerosol forcing emulator (EVA_H): Comparison with interactive stratospheric aerosol models. J. Geophys. Res.: Atm., 125: e2019JD031303.

Balsamo, G., A. Beljaars, K. Scipal, P. Viterbo, B. van den Hurk, M. Hirschi, and A. K. Betts (2009). A revised hydrology for the ECMWF model: Verification from field site to terrestrial water storage and impact in the integrated forecast system. J. Hydrometeor., 10: 623–643, doi:10.1175/2008JHM1068.1.

Batté, L. and Déqué, M. (2016). Randomly correcting model errors in the ARPEGE-Climate v6.1 component of CNRM-CM : applications for seasonal forecasts. Geosci. Mod. Dev., 9: 2055-2076, doi:10.5194/gmd-9-2055-2016

Batté, L., Välisuo I., Chevallier M., Acosta Navarro J.C., Ortega P. and Smith D. (2020). Summer predictions of Arctic sea ice edge in multi-model seasonal re-forecasts. Clim. Dyn., 54: 5013–5029. doi: 10.1007/s00382-020-05273-8

Bilbao, R., Wild, S., Ortega, P., Acosta-Navarro, J., Arsouze, T., Bretonnière, P.-A., et al. (2021). Assessment of a full-field initialised decadal climate prediction system with the CMIP6 version of EC-Earth. Earth Syst. Dynam., 12: 173–196, https://doi.org/10.5194/esd-12-173-2021.

Boer, G. J., Smith, D. M., Cassou, C., Doblas-Reyes, F., Danabasoglu, G., Kirtman, B., et al. (2016). The Decadal Climate Prediction Project (DCPP) contribution to CMIP6, Geosci. Mod. Dev., 9: 3751–3777.

DallaSanta, K., and Polvani, L.M. (2022). Volcanic stratospheric injections up to 160 tg(s) yield a eurasian winter warming indistinguishable from internal variability. Atmos. Chem. Phys., 22: 8843–8862, https://doi.org/10.5194/acp-22-8843-2022.

Decharme, B., Delire, C., Minvielle, M., Colin, J., Vergnes, J.-P., Alias, A., et al. (2019). Recent changes in the ISBA-CTRIP land surface system for use in the CNRM-CM6 climate model and in global off-line hydrological applications. Journal of Advances in Modeling Earth Systems, 11, 1207– 1252. https://doi.org/10.1029/2018MS001545

Dee, D., et al. (2011). The ERA-Interim reanalysis: Configuration and performance of the data assimilation system. Quart. J. Roy. Meteor. Soc., 137, 553–597, doi:10.1002/qj.828.

Döscher, R., Acosta, M., Alessandri, A., Anthoni, P., Arneth, A., et al. (2022). The EC-Earth3 Earth System Model for the Climate Model Intercomparison Project 6, Geosci. Model Dev., 15, 2973–3020, https://doi.org/10.5194/gmd-15-2973-2022.

Driscoll, S., Bozzo, A., Gray, L. J., Robock, A., and Stenchikov, G. (2012). Coupled Model Intercomparison Project 5 (CMIP5) simulations of climate following volcanic eruptions, J. Geophys. Res., 117: D17105.

Hobeichi, S., Abramowitz, G., and Evans, J. P. (2021). Robust historical evapotranspiration trends across climate regimes, Hydrol. Earth Syst. Sci., 25: 3855–3874, https://doi.org/10.5194/hess-25-3855-2021.

Hersbach, H, Bell, B, Berrisford, P, et al. (2020). The ERA5 global reanalysis. Q J R Meteorol Soc., 146: 1999–2049. https://doi.org/10.1002/qj.3803

Hermanson, L., Bilbao, R., Dunstone, N., Ménégoz, M., Ortega, P., Pohlmann, H., et al. (2020) Robust Multiyear Climate Impacts of Volcanic Eruptions in Decadal Prediction Systems. J. Geophys. Res.: Atm., 125: e2019JD031739. doi: 10.1029/2019jd031739.

Johnson, S. J., Stockdale, T. N., Ferranti, L., Balmaseda, M. A., Molteni, F., Magnusson, L., et al. (2019). SEAS5: the new ECMWF seasonal forecast system. Geosci. Mod. Dev., 12: 1087-1117. https://doi.org/10.5194/gmd-12-1087-2019

Khodri, M., Izumo, T., Vialard, J. et al. (2017). Tropical explosive volcanic eruptions can trigger El Niño by cooling tropical Africa. Nat Commun 8: 778 . https://doi.org/10.1038/s41467-017-00755-6

Liu, Q., L. Wang, Y. Qu, N. Liu, S. Liu, H. Tang, and S. Liang (2013). Preliminary evaluation of the long-term GLASS albedo product. Int. J. Digit. Earth, 6 (sup1): 69–95, doi:10.1080/ 17538947.2013.804601.

Marshall L.R., Maters, E.C., Schmidt, A., Timmreck, C., Robock, A., and Toohey, M. (2022). Volcanic effects on climate: recent advances and future avenues. Bull. Volcan. 84:131.

Ménégoz, M., Bilbao, R., Bellprat, O., Guemas, V., and Doblas-Reyes, F. (2018). Forecasting the climate response to volcanic eruptions: prediction skill related to stratospheric aerosol forcing. Environ. Res. Lett. 13(6): 64,022. https://doi.org/10.1007/s00382-017-3986-1

Swingedouw, D., Mignot, J., Ortega, P., Khodri, M., Menegoz, M., Cassou, C., and Hanquiez, V. (2017). Impact of explosive volcanic eruptions on the main climate variability modes. Global and Planetary Change, 150: 24–45.

Toohey, M., Stevens, B., Schmidt, H., and Timmreck, C. (2016). Easy Volcanic Aerosol (EVA v1.0): An idealized forcing generator for climate simulations. Geosci. Model Dev., 2016, 1– 40.

Voldoire, A., Saint-Martin, D., Sénési, S., Decharme, B., Alias, A., Chevallier, M., et al. (2019). Evaluation of CMIP6 DECK experiments with CNRM-CM6-1. J. Adv. Model. Earth Syst., 11, 2177– 2213. https://doi.org/10.1029/2019MS001683

Zanchettin, D., Khodri, M., Timmreck, C., Toohey, M., Schmidt, A., Gerber, E. P., et al. (2016) The Model Intercomparison Project on the climatic response to Volcanic forcing (VolMIP): experimental design and forcing input data for CMIP6, Geosci. Model Dev., 9: 2701–2719, https://doi.org/10.5194/gmd-9-2701-2016.

Zhu, Z., Bi, J., Pan, Y., Ganguly, S., Anav, A., Xu, L., et al. (2013). Global Data Sets of Vegetation Leaf Area Index (LAI)3g and Fraction of Photosynthetically Active Radiation (FPAR)3g Derived from Global Inventory Modeling and Mapping Studies (GIMMS) Normalized Difference Vegetation Index (NDVI3g) for the Period 1981 to 2011, Remote Sens., 5: 927–948.

Articles in preparation

Alessandri, A. and co-authors (in prep.) Enhancement of seasonal climate prediction in ECMWF SEAS5 by representing realistic vegetation-cover variability.

Bilbao, R. and co-authors (in prep.) Impact of volcanic eruptions in CMIP6 decadal prediction systems: a multi-model analysis.

Document History

Version	Author(s)	Date	Changes
1.0	Lauriane Batté (MF)	19/10/2022	First version complete for internal review
1.1	Lauriane Batté (MF)	26/10/2022	Rephrasing of some conclusions and changes in document organization following feedback from internal review

Internal Review History

Internal Reviewers	Date	Comments
Pablo Ortega (BSC)	19/10/2022	

Estimated Effort Contribution per Partner

Partner	Effort
MF	5
BSC	7
ECMWF	
ISAC-CNR	
Total	12